QUANTUM SIMULATION

Creation of a low-entropy quantum gas of polar molecules in an optical lattice

Steven A. Moses, Jacob P. Covey, Matthew T. Miecnikowski, Bo Yan,* Bryce Gadway,† Jun Ye,‡ Deborah S. Jin‡

Ultracold polar molecules, with their long-range electric dipolar interactions, offer a unique platform for studying correlated quantum many-body phenomena. However, realizing a highly degenerate quantum gas of molecules with a low entropy per particle is challenging. We report the synthesis of a low-entropy quantum gas of potassium-rubidium molecules (KRb) in a three-dimensional optical lattice. We simultaneously load into the optical lattice a Mott insulator of bosonic Rb atoms and a single-band insulator of fermionic K atoms. Then, using magnetoassociation and optical state transfer, we efficiently produce ground-state molecules in the lattice at those sites that contain one Rb and one K atom. The achieved filling fraction of 25% should enable future studies of transport and entanglement propagation in a many-body system with long-range dipolar interactions.

Polar molecules are an ideal candidate system for studying spin physics and emulating quantum magnetism (*1*–*3*). However, low temperatures and long lifetimes are required. Ultracold fermionic KRb molecules have been created at a temperature T close to the Fermi temperature T_F (*4*), but cooling a trapped molecular gas deeply into quantum degeneracy has yet to be demonstrated (*5*–*7*). For KRb, the biggest problem is that two molecules can chemically react, which limits the lifetime of the trapped gas (*8*). Furthermore, the chemical reaction rate increases in an applied electric field because of the attractive part of the dipole-dipole interactions (*8*). A solution to this problem is to confine the molecules in a deep optical lattice in order to restrict collisions (*9*–*11*). In particular, the lifetime of ground-state molecules in a deep three-dimensional (3D) lattice was demonstrated to be longer than 20 s and limited by off-resonant scattering of the lattice light (*11*). With the chemical reactions mitigated, the remaining challenge is to create a low-entropy system, which in the lattice corresponds to increasing the filling fraction. Here, we report the realization of a high-filling, low-entropy quantum gas of ground-state molecules in a deep 3D lattice using a quantum synthesis approach.

Simulating quantum many-body physics with lattice-confined atoms requires a filling near unity and correspondingly low entropy (*12*). This condition can be substantially relaxed with polar molecules thanks to their long-range dipolar interactions, which allow for a decoupling of spin and motion so that only the spin entropy, which can be prepared to be near zero, is relevant (*3*). This was recently demonstrated in (*13*, *14*), where a spin-½ system was realized by encoding spin in the rotational degree of freedom of the KRb molecules. At dilute lattice fillings, spin exchange via dipolar interactions was observed in the density-dependent decay of, and oscillations in, the spin coherence. To go beyond this observation and explore problems such as the spin-½ Hamiltonian for quantum magnetism (*15*–*21*), the propagation of excitations and the growth of entanglement and correlations (*22*, *23*), many-body localization (*24*), exotic quantum phases (*25*–*29*), and spin-orbit coupling with molecules (*30*), higher lattice fillings will be essential. Determining what constitutes high lattice filling depends on the specific experiment in question; one benchmark is the percolation threshold, which for an infinite simple cubic lattice with nearest-neighbor interactions corresponds to a filling of ~0.3 (*31*). Because of the molecules' long-range interactions and the finite system size, a filling near this percolation threshold is sufficient for exploring dynamics such as the propagation of excitations.

Our strategy for realizing higher lattice fillings for polar molecules is to take advantage of the precise experimental control available for manipulating the initial atomic quantum gas mixture in a 3D lattice (*32*, *33*). Specifically, one needs to prepare a low-entropy state of two atomic species in the lattice and combine this with efficient molecule production. We use magnetoassociation to first create very weakly bound Feshbach molecules followed by optical transfer to the molecular ro-vibrational ground state. Previously, we showed that the conversion efficiency from atoms to Feshbach molecules is high (87 ± 13%) for lattice sites containing exactly one Rb atom and one K atom (*11*). In addition, previous measurements of inelastic collisional loss rates for Feshbach molecules with K or Rb atoms (*8*, *34*) suggest that having an extra atom on a lattice site will be detrimental to molecule production at that site.

The basic scheme is illustrated in Fig. 1. By loading a nearly pure Bose-Einstein condensate (BEC) of Rb atoms into a 3D optical lattice, we achieve a Mott insulator (MI) state, where repulsive interactions between the Rb atoms drive a transition to a state that has an integer number of particles per site (*35*). The lattice depth is subsequently increased to pin the Rb atoms. The initial BEC density should be low enough to avoid having multiply occupied sites. For spin-polarized fermionic K atoms, Pauli blocking will prevent any site from having more than one K atom if the atoms are all prepared in the lowest band. The optimum case is a K band insulator (*36*, *37*) of one atom per site, which requires starting with a relatively large initial K density. Creating both insulators simultaneously is very challenging. The densities of both species should be ~$(\lambda/2)^{-3}$

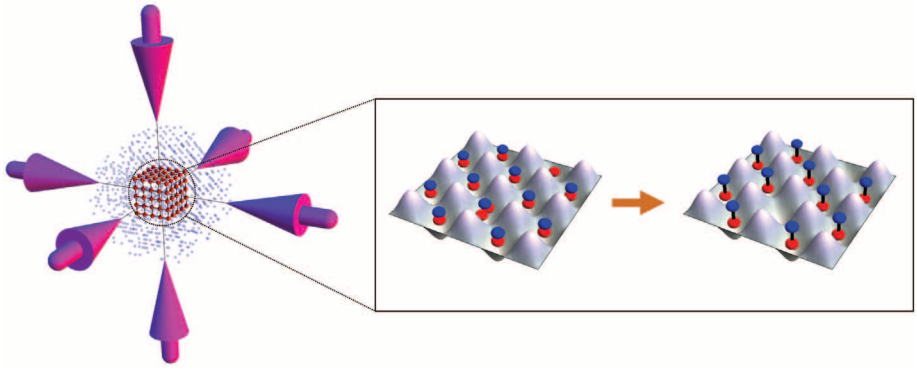

Fig. 1. Quantum synthesis for creating polar molecules. Left: We load K (blue) and Rb (red) atoms into a 3D optical lattice, with many more K atoms than Rb atoms. In the center of the lattice where the two atom clouds overlap, we realize a Rb Mott insulator and a K single-band insulator, each with near-unity filling. Right: Sites with one Rb and one K have a high probability of producing molecules, whereas sites with multiple Rb or with only a single atomic species do not yield molecules.

JILA, National Institute of Standards and Technology and University of Colorado, and Department of Physics, University of Colorado, Boulder, CO 80309, USA. *Present address: Department of Physics, Zhejiang University, Hangzhou 310027, China. †Present address: Department of Physics, University of Illinois at Urbana-Champaign, Urbana, IL 61801, USA. ‡Corresponding author. E-mail: ye@jila.colorado.edu (J.Y.); jin@jilau1.colorado.edu (D.S.J.)

prior to loading the lattice, where $\lambda/2$ is the lattice spacing. When loading both species into a common optical lattice, we thus need to work with a Rb BEC with small atom number and a degenerate Fermi gas with large atom number. The Rb MI must be well spatially overlapped with the center of the much larger K distribution. We also need to preserve the high filling of each atomic species in the presence of the other. Finally, any excess atoms should be removed quickly from the lattice after the molecule production.

To prepare the atomic quantum gases, we evaporate Rb in the $|1,1\rangle$ state and sympathetically cool K in the $|^9/_2, -^9/_2\rangle$ state in a crossed-beam optical dipole trap with a wavelength $\lambda = 1064$ nm. Here, the atomic hyperfine states are denoted by $|F, m_F\rangle$, where F is the total atomic spin and m_F is its projection. The evaporation is performed at a magnetic field B of 540 G, where the interspecies scattering length a_{KRb} is $-100a_0$, with a_0 the Bohr radius. This field provides for modest interspecies interactions while being close to an interspecies Feshbach resonance (*38*) at $B_0 = 546.6$ G that is used for tuning interactions as well as for molecule creation. The final optical trap is cylindrically symmetric with a typical axial trap frequency of $\omega_z = 2\pi \times 180$ Hz (along gravity) and a radial trap frequency of $\omega_r = 2\pi \times 25$ Hz for Rb. The measured trap frequencies for K are $2\pi \times 260$ Hz and $2\pi \times 30$ Hz. The larger vertical trap frequency helps prevent separation of the Rb and K clouds due to gravitational sag. Immediately after the evaporation, we turn off the interspecies interactions by ramping B to 543.6 G where $a_{KRb} = 0$. At this point, we have a Fermi gas of 1×10^5 to 2×10^5 K atoms and a nearly pure Rb BEC with 10^3 to 10^4 atoms. Once Rb condenses, it no longer thermalizes efficiently with K, and as a result the temperature of the K gas does not reach below $T/T_F \approx 0.3$. We then smoothly turn on, in 150 ms, three retro-reflected beams with $\lambda = 1064$ nm that form a cubic optical lattice. Two of the lattice beams are in the horizontal plane; the third beam is at an angle of 6° from vertical. The final lattice depth is between 20 and 25 E_R^{Rb}, where $E_R^{Rb} = \hbar^2k^2/2m$ is the recoil energy for Rb, $k = 2\pi/\lambda$, $\hbar$ is the Planck constant divided by 2π, and m is the mass of the Rb atom.

We image the atom clouds, either in situ in the lattice or after a time-of-flight (TOF) expansion, using resonant absorption imaging with a probe beam that propagates along the vertical direction. As the lattice depth is increased beyond the superfluid-MI transition of the Rb gas, coherent matter wave interference disappears (Fig. 2A). Figure 2B shows a TOF image of 1.8×10^5 K atoms, where the lattice was turned off more slowly for band mapping (*39*). A trace through this image along the direction of one of the horizontal lattice beams, which is rotated by roughly 45° with

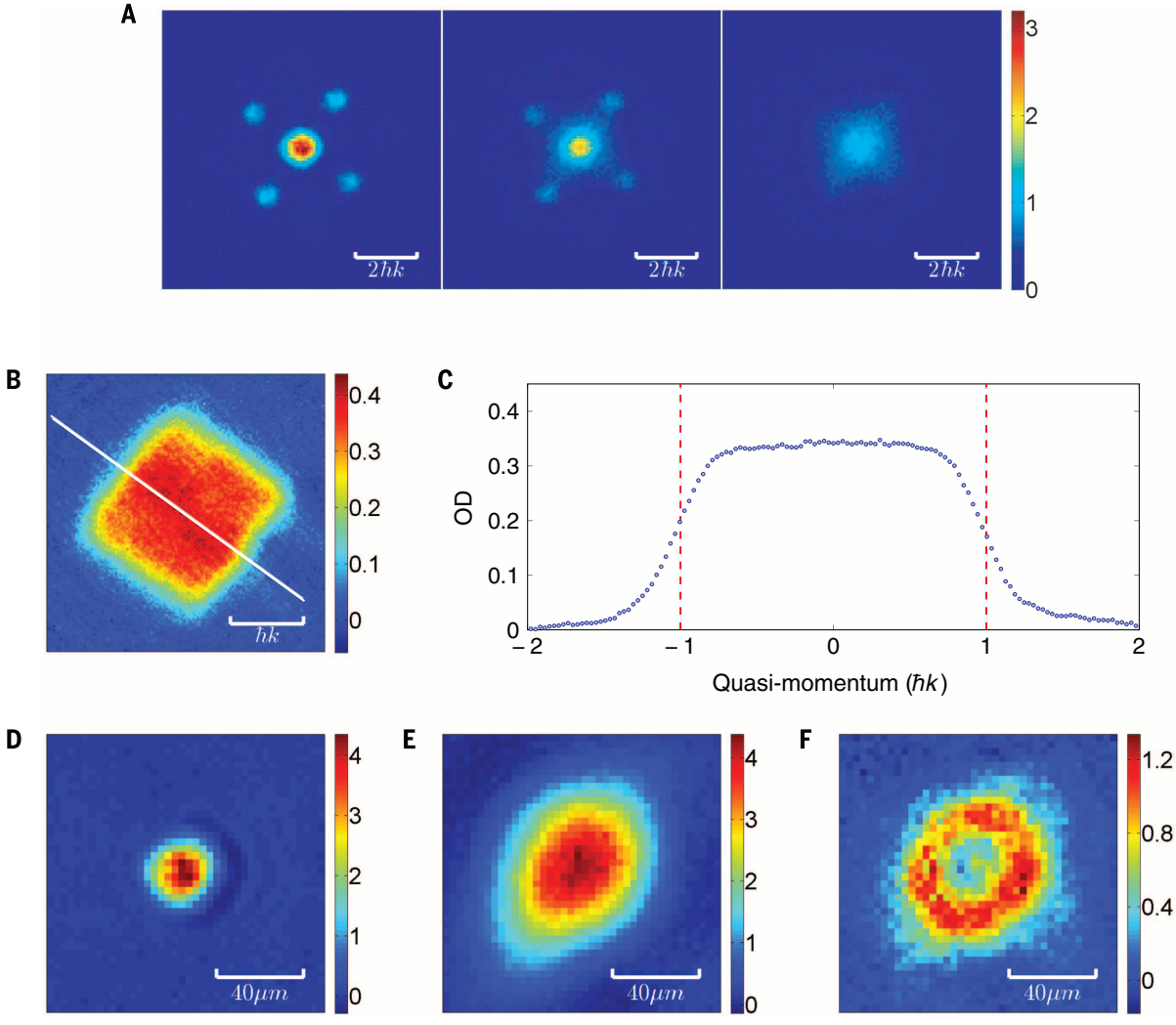

Fig. 2. Imaging of Rb and K clouds. (**A**) The superfluid–Mott insulator transition for Rb, with ~8×10^4 atoms. The images were taken with TOF = 8 ms; the final lattice depth is 12, 17, or 22 E_R^{Rb} from left to right. The optical depth (OD) for each image is indicated by the color bar to the right of the image; scale bar units refer to momentum. (**B**) Band mapping of K, imaged after 11.5 ms of expansion. The white line shows the direction of the cut shown in (C). (**C**) Cut through the K band-mapping image, showing OD versus quasi-momentum. (**D**) In situ image of 2×10^4 Rb atoms. (**E**) In situ image of 1.8×10^5 K atoms. (**F**) In situ image of the K cloud after initiating loss due to K-Rb inelastic collisions. The resulting hole in the K cloud demonstrates good initial spatial overlap with the Rb cloud in all three directions.

respect to the camera axes (and averaged along the other direction), shows that most of the atoms are in the lowest band (Fig. 2C). In situ images of Rb (Fig. 2D) and K (Fig. 2E) reveal that the Rb cloud is much smaller than the K cloud. To verify that the clouds are spatially overlapped, we used a radio-frequency (RF) pulse to transfer the Rb atoms to the $|2,2\rangle$ state in order to induce spin-changing collisions that result in loss of K and Rb atoms on the same lattice site. The resultant hole in the K distribution (Fig. 2F) clearly demonstrates that the clouds are overlapped in the trap.

We determine the peak filling fraction from fits to the measured atomic distributions. We fit the K Fermi gas with a Gaussian. In this case, the peak filling is

$$f_K = \frac{N(\lambda/2)^3}{(2\pi)^{3/2}\sigma_x\sigma_y\sigma_z} \quad (1)$$

where N is the number of atoms and σ_x, σ_y, and σ_z are the Gaussian root mean square widths. The Rb MI is better described by a Thomas-Fermi (TF) distribution (*40*), and the peak filling is

$$f_{Rb} = \frac{15N(\lambda/2)^3}{8\pi R_x R_y R_z} \quad (2)$$

where R_x, R_y, and R_z are the TF radii. We image the gas along z, so we determine the radial size. The vertical size is smaller by a factor of $A = 6.4 \pm 0.1$, which is measured for a thermal gas of Rb in the combined potential of the optical trap and lattice.

Figure 3A shows f_{Rb} versus Rb number. For a comparison to the data, we calculate the $T = 0$ MI distribution for our trap, convolve this distribution with a Gaussian filter to account for the finite imaging resolution, bin the data into pixels, and then fit with a TF distribution (*41*). For very small samples, the size of the cloud is about twice the imaging resolution. The data correspond well to the $T = 0$ calculation, and from this comparison, we infer that the $N = 1$ Rb MI occurs for fewer than 5000 atoms in our trap.

Figure 3B shows f_K versus K number in a 23 E_R^{Rb} lattice. Given the different mass and ac polarizability for K, this is equivalent to only 9 E_R^K, where E_R^K is the recoil energy for K atoms. We find that f_K rises with increasing K atom number (blue points) and saturates around 80% for K numbers ≥1 × 10^5. For these data, T/T_F decreases with increasing K number (red points). The saturation of f_K is consistent with the onset of a band insulator in the center of the lattice.

The data in Fig. 3, A and B, show that to achieve optimal molecule production, the initial BEC should have fewer than 5000 atoms for a MI with mostly one atom per site, whereas the Fermi gas should have more than 10^5 atoms to reach the band insulating limit. When loading both atom species at very low temperatures, one might expect attractive interactions to enhance the overlap between the two species (*33*, *42*). For the temperatures achieved in our experiment, the hotter K gas affects the filling of Rb, and we find empirically that turning off interactions by going to $a_{KRb} = 0$ is optimum (*41*). To illustrate this effect, fig. S1 shows how f_{Rb} and the initial BEC fraction depend on a_{KRb}.

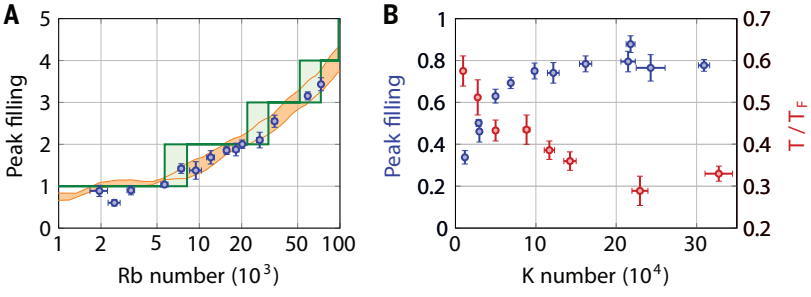

Fig. 3. Peak filling for Rb and K clouds. (**A**) f_{Rb} (blue points) versus Rb number. The cloud size was extracted from a TF fit to the in situ image; the Rb number was extracted from the in situ image or from a Gaussian fit to the cloud after a few milliseconds of free expansion. The filling was computed according to Eq. 2. The green staircase displays the calculated peak occupancy for a $T = 0$ distribution (*41*). The total harmonic confinement (including the lattice light) is represented by $\omega_r = 2\pi \times (38 \pm 2)$ Hz and $\omega_z = (6.4 \pm 0.1)\omega_r$. The orange band shows a fit to the calculated density distribution, accounting for finite imaging resolution and pixelation present in the experiment. (**B**) Peak filling f_K versus K number for a lattice depth of 9 E_R^K (blue points), indicating the onset of a K band insulator for $N_K > 10^5$. The red points show the measured T/T_F of the initial K gas before loading the lattice.

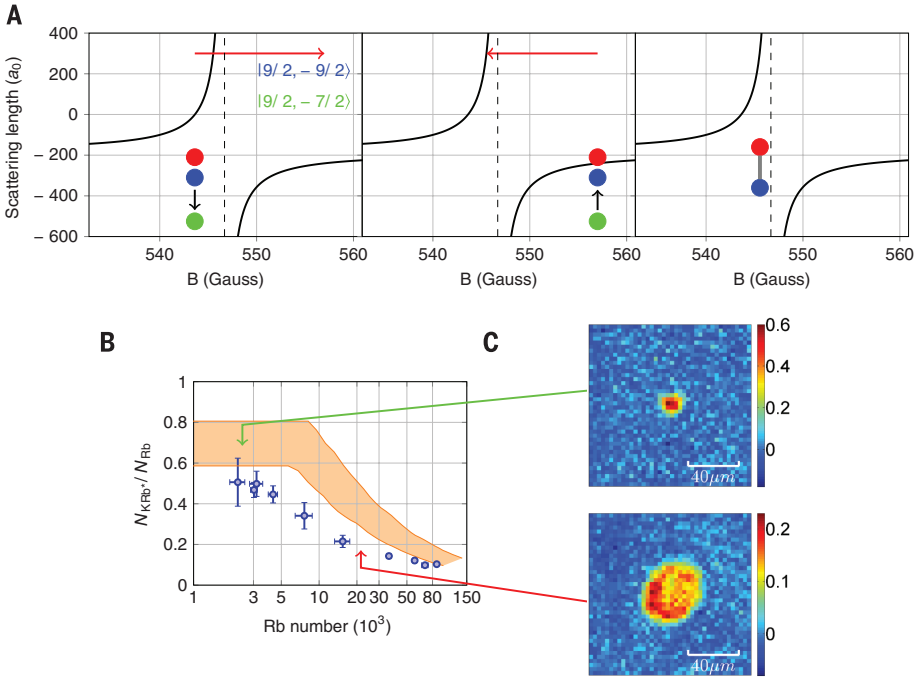

Fig. 4. Molecule formation. (**A**) The interspecies Feshbach resonance. The atoms are loaded into the lattice at $a_{KRb} = 0$. The K atoms are then transferred to a hyperfine state ($|9/2, -7/2\rangle$) that does not participate in the resonance, and B is swept above the resonance. After transferring K back to the $|9/2, -9/2\rangle$ state, magnetoassociation proceeds by sweeping B from above to below the resonance (center and right panels). The Feshbach molecules are then transferred to the absolute ground state via STIRAP. (**B**) Fraction of Rb atoms converted to Feshbach molecules. The orange-shaded region shows the expected fraction of Rb atoms that are on a site with exactly one Rb atom and one K atom. (**C**) In situ images of ground-state KRb molecules after a 40-ms hold in the lattice. For low initial Rb number (top image, average of three repeated experiments), we find a filling fraction of 25 ± 4%. For higher Rb number (bottom image, average of seven shots), we observe a hole in the center of the molecular distribution, and the filling is much lower.

The first step in creating ground-state molecules is magnetoassociation, which consists of adiabatically sweeping B across the K-Rb Feshbach resonance from high to low field (Fig. 4A). However, starting from $a_{KRb} = 0$, which occurs for $B < B_0$, we first need to jump B to the high-field side of the resonance. This jump should be diabatic in order to avoid promoting atoms to higher lattice bands (*39*); however, the high local atom densities in the lattice make it difficult to sweep the field fast enough. To overcome this problem, we use an RF pulse to transfer the K atoms to a spin state, $|^9/_2, -^7/_2\rangle$, that does not experience the 546.6 G resonance. After ramping B above B_0, we transfer the K atoms back to the $|^9/_2, -^9/_2\rangle$ state and then proceed with magnetoassociation. We find that applying these RF transitions improves the final filling of ground-state molecules by 60% relative to the case of not doing these RF transitions.

Figure 4B shows the measured fraction of the Rb number, N_{Rb}, that is converted to Feshbach molecules (blue points). Because we operate with many more K atoms than Rb atoms, a large background of K atoms remains after making molecules. To determine the number of Feshbach molecules N_{KRb^*}, we use RF to transfer the background K atoms to another spin state before dissociating the molecules and imaging the resulting K (*41*). For comparison with the data, the shaded band in Fig. 4B shows the product of the measured $f_K = 0.80 \pm 0.05$, the calculated fraction of Rb atoms of a $T = 0$ MI that are on singly occupied sites, and the conversion efficiency of preformed pairs reported in (*11*). We find that the trend of the calculation matches the data, with the conversion efficiency decreasing for higher Rb number. This is consistent with the expectation that molecules are not produced on sites that have more than one Rb atom. The data lie slightly below the calculation; possible explanations for this include finite temperature effects on the MI, leading to fewer singly occupied sites, or reduced conversion efficiency for sites with one Rb and one K atom. For small Rb numbers, we find that N_{KRb^*}/N_{Rb} exceeds 50%.

As a last step, we use stimulated Raman adiabatic passage (STIRAP) to transfer the Feshbach molecules to their ro-vibrational ground state (*4*). The typical efficiency of this transfer is 89 ± 4%. After STIRAP, we apply resonant light pulses to remove all unpaired atoms from the lattice; without this step, the molecule lifetime in the lattice is only a few milliseconds, which we attribute to K tunneling followed by molecule-atom chemical reactions (*8*). After holding the ground-state molecules in the lattice for 40 ms, we take in situ images of the molecule distribution by reversing the STIRAP process, dissociating the Feshbach molecules, and then imaging the K atoms. Figure 4C shows images of the ground-state molecules in the lattice for cases of high (top) and low conversion (bottom), corresponding to starting with roughly 2500 and 25,000 Rb atoms, respectively. The bottom image exhibits a central hole in the molecule distribution, which is consistent with the central lattice sites containing multiple Rb atoms and therefore not producing molecules.

For the higher-conversion case, we perform a TF fit to the ground-state molecular distribution. From the fit we find 7.9 (±0.5) × 10^2 molecules with a TF radius of 12.0 (±0.2) μm. This gives $f_{mol} = 0.27 \pm 0.02$. As an alternative approach, we can determine the filling by comparing the width of the molecular cloud to that of our simulated $T = 0$ Rb distribution and assuming a uniform conversion efficiency of Rb into molecules. The molecules are best described by a distribution that corresponds to an initial Rb number of 3.2 (±0.4) × 10^3. Taking the ratio of the measured number of molecules to this Rb number, we find $f_{mol} = 0.25 \pm 0.04$, which is consistent with the other method. From the product of the previous measurements, namely f_{Rb}, N_{KRb^*}/N_{Rb}, and the STIRAP efficiency, one might expect $f_{mol} \approx 0.35$. We attribute the lower measured filling to molecular loss caused by the atom removals.

Given the ac polarizability (*43*) and mass of the ground-state molecules, a 25 E_R^{Rb} lattice corresponds to 62 E_R^{KRb}, where E_R^{KRb} is the recoil energy for a KRb molecule. The tunneling rate for molecules is therefore negligible, and the lifetime is long and limited by single-photon scattering (*11*). In this case, the entropy per molecule can be estimated from the filling in the lattice, with some assumption about the shape of the distribution. Our approach likely leads to a molecular distribution that is much more homogeneous than the alternative approach of adiabatically loading a Fermi gas of molecules into the lattice. The K Fermi gas is homogeneous within the confines of the Rb MI, and the entropy per particle in this region is roughly that of a lattice system with a uniform filling of 80%, which is about 0.6 k_B. For an average filling of f in a uniform lattice, the entropy per particle is $(-k_B/f)[f \ln(f) + (1-f)\ln(1-f)]$ (*44*). Similarly, for $f_{mol} = 25\%$, the entropy per molecule is 2.2 k_B. For comparison, the lowest entropy we have achieved in a harmonic trap is about 6 k_B per molecule, corresponding to $T/T_F \approx 1$.

The system realized here is appropriately sized for imaging with quantum gas microscopy (*45*–*47*), where dynamics associated with percolation can be investigated. More generally, this work elucidates the many challenges in, and extends the experimental toolbox for, synthesizing ultracold molecule systems that can realize novel quantum many-body behavior.

REFERENCES AND NOTES

1. A. Micheli, G. K. Brennen, P. Zoller, *Nat. Phys.* **2**, 341–347 (2006).
2. R. Barnett, D. Petrov, M. Lukin, E. Demler, *Phys. Rev. Lett.* **96**, 190401 (2006).
3. K. R. A. Hazzard, S. R. Manmana, M. Foss-Feig, A. M. Rey, *Phys. Rev. Lett.* **110**, 075301 (2013).
4. K.-K. Ni *et al.*, *Science* **322**, 231–235 (2008).
5. T. Takekoshi *et al.*, *Phys. Rev. Lett.* **113**, 205301 (2014).
6. P. K. Molony *et al.*, *Phys. Rev. Lett.* **113**, 255301 (2014).
7. J. W. Park, S. A. Will, M. W. Zwierlein, *Phys. Rev. Lett.* **114**, 205302 (2015).
8. S. Ospelkaus *et al.*, *Science* **327**, 853–857 (2010).
9. H. P. Büchler *et al.*, *Phys. Rev. Lett.* **98**, 060404 (2007).
10. M. H. G. de Miranda *et al.*, *Nat. Phys.* **7**, 502–507 (2011).
11. A. Chotia *et al.*, *Phys. Rev. Lett.* **108**, 080405 (2012).
12. I. Bloch, J. Dalibard, S. Nascimbene, *Nat. Phys.* **8**, 267–276 (2012).
13. B. Yan *et al.*, *Nature* **501**, 521–525 (2013).
14. K. R. A. Hazzard *et al.*, *Phys. Rev. Lett.* **113**, 195302 (2014).
15. A. V. Gorshkov *et al.*, *Phys. Rev. Lett.* **107**, 115301 (2011).
16. A. de Paz *et al.*, *Phys. Rev. Lett.* **111**, 185305 (2013).
17. T. Fukuhara *et al.*, *Nat. Phys.* **9**, 235–241 (2013).
18. P. Richerme *et al.*, *Nature* **511**, 198–201 (2014).
19. P. Jurcevic *et al.*, *Nature* **511**, 202–205 (2014).
20. J. Cai, A. Retzker, F. Jelezko, M. B. Plenio, *Nat. Phys.* **9**, 168–173 (2013).
21. S. Ravets *et al.*, *Nat. Phys.* **10**, 914–917 (2014).
22. K. R. A. Hazzard *et al.*, *Phys. Rev. A* **90**, 063622 (2014).
23. J. Schachenmayer, B. P. Lanyon, C. F. Roos, A. J. Daley, *Phys. Rev. X* **3**, 031015 (2013).
24. N. Y. Yao *et al.*, *Phys. Rev. Lett.* **113**, 243002 (2014).
25. K. A. Kuns, A. M. Rey, A. V. Gorshkov, *Phys. Rev. A* **84**, 063639 (2011).
26. M. Knap, E. Berg, M. Ganahl, E. Demler, *Phys. Rev. B* **86**, 064501 (2012).
27. S. R. Manmana, E. M. Stoudenmire, K. R. A. Hazzard, A. M. Rey, A. V. Gorshkov, *Phys. Rev. B* **87**, 081106 (2013).
28. L. He, W. Hofstetter, *Phys. Rev. A* **83**, 053629 (2011).
29. N. Y. Yao *et al.*, *Phys. Rev. Lett.* **110**, 185302 (2013).
30. S. V. Syzranov, M. L. Wall, V. Gurarie, A. M. Rey, *Nat. Commun.* **5**, 5391 (2014).
31. D. Stauffer, A. Aharon, *Introduction to Percolation Theory* (Taylor and Francis, London, revised ed. 2, 1994).
32. B. Damski *et al.*, *Phys. Rev. Lett.* **90**, 110401 (2003).
33. J. K. Freericks *et al.*, *Phys. Rev. A* **81**, 011605 (2010).
34. J. J. Zirbel *et al.*, *Phys. Rev. Lett.* **100**, 143201 (2008).
35. I. Bloch, J. Dalibard, W. Zwerger, *Rev. Mod. Phys.* **80**, 885–964 (2008).
36. U. Schneider *et al.*, *Science* **322**, 1520–1525 (2008).
37. R. Jördens, N. Strohmaier, K. Günter, H. Moritz, T. Esslinger, *Nature* **455**, 204–207 (2008).
38. C. Klempt *et al.*, *Phys. Rev. A* **78**, 061602 (2008).
39. M. Köhl, H. Moritz, T. Stöferle, K. Günter, T. Esslinger, *Phys. Rev. Lett.* **94**, 080403 (2005).
40. B. DeMarco, C. Lannert, S. Vishveshwara, T.-C. Wei, *Phys. Rev. A* **71**, 063601 (2005).
41. See supplementary materials on *Science* Online.
42. S. Sugawa *et al.*, *Nat. Phys.* **7**, 642–648 (2011).
43. B. Neyenhuis *et al.*, *Phys. Rev. Lett.* **109**, 230403 (2012).
44. D. Budker, D. Kimball, D. Demille, *Atomic Physics: An Exploration Through Problems and Solutions* (Oxford Univ. Press, Oxford, ed. 2, 2008).
45. W. S. Bakr, J. I. Gillen, A. Peng, S. Fölling, M. Greiner, *Nature* **462**, 74–77 (2009).
46. J. F. Sherson *et al.*, *Nature* **467**, 68–72 (2010).
47. N. Gemelke, X. Zhang, C.-L. Hung, C. Chin, *Nature* **460**, 995–998 (2009).

ACKNOWLEDGMENTS

We thank Z. Fu for experimental assistance and M. Wall, A. Safavi, K. Hazzard, and A. M. Rey for many useful discussions. Supported by a National Defense Science and Engineering graduate fellowship (J.P.C.), the National Institute of Standards and Technology, the Air Force Office of Scientific Research Multidisciplinary University Research Initiative (MURI), the Army Research Office MURI, and NSF grant 1125844.

SUPPLEMENTARY MATERIALS

www.sciencemag.org/content/350/6261/659/suppl/DC1
Materials and Methods
Fig. S1

24 May 2015; accepted 30 September 2015
10.1126/science.aac6400

Creation of a low-entropy quantum gas of polar molecules in an optical lattice

Steven A. Moses *et al.*

Science **350**, 659 (2015);
DOI: 10.1126/science.aac6400